Nanoscale

Insights into the Thermal and Chemical Stability of Multilayered V2CTx MXene Under Different Environments

Journal:	*Nanoscale*
Manuscript ID	NR-ART-04-2019-003020
Article Type:	Paper
Date Submitted by the Author:	08-Apr-2019
Complete List of Authors:	Thakur, Raj ; Auburn University, Chemical Engineering VahidMohammadi, Armin; Auburn University, Materials Engineering Moncada, Jorge; Auburn University, Chemical Engineering Adams, Reid ; Auburn University, Chemical Engineering Chi, Mingyang ; Auburn University, Chemical Engineering Tatarchuk, Bruce; Auburn University, Chemical Engineering Beidaghi, Majid; Auburn University, Materials Engineering Carrero, Carlos A.; Auburn University, Chemical Engineering

SCHOLARONE™
Manuscripts

Insights into the Thermal and Chemical Stability of Multilayered V_2CT_x MXene Under Different Environments

Raj Thakur [†], Armin VahidMohammadi [‡], Jorge Moncada [†], Reid Adams [†], Mingyang Chi [†], Bruce Tatarchuk [†], Majid Beidaghi [‡*], Carlos A. Carrero [†*]

† Department of Chemical Engineering, Auburn University, Auburn, Alabama 36830, United States
‡ Department of Materials Engineering, Auburn University, Auburn, Alabama 36830, United States
* Corresponding authors: cac0134@auburn.edu, mzb0088@auburn.edu

Abstract

We report on the thermal stability of multilayered V_2CT_x MXene under different atmospheres by combining *in situ* Raman Spectroscopy with *ex situ* X-ray Diffraction (XRD), X-ray Photoelectron Spectroscopy (XPS), and Scanning Electron Microscopy (SEM) in order to elucidate and monitor molecular, electronic, and structural changes of both the surface and bulk of the V_2CT_x MXene which has recently received much attention. The MXene samples were heated up to 600 °C under inert (N_2), oxidative (CO_2, air), and reductive (H_2) environments with similar conditions. *In situ* Raman showed that the V=O vibration for two-dimensional vanadia is preserved up to 600 °C under N_2, while its intensity reduces under H_2. When heated above 300 °C under either CO_2 or air, V_2CT_x slightly oxidizes or transform into V_2O_5, respectively. Furthermore, SEM revealed the persistence of an accordion-like layered structure for the MXene under N_2 and H_2, while under CO_2 and air the layered structure collapses and form VO_2 (V^{4+}) and V_2O_5 (V^{5+}) crystals, respectively. XPS reveals that, regardless of the gas, surface V species oxidize above 300 °C during the dehydration process. Finally, we demonstrated that the partial dehydration of V_2CT_x results in the partial oxidation of the material, and the total dehydration is achieved once 700 ^{0}C is reached. We believe that our methodology is a unique alternative to tune the dehydration, oxidation, and properties of V_2CT_x, which allows for the expansion of MXenes' applications.

Keywords: MXene, V_2CT_x, 2D materials, thermal stability, environments, catalyst.

1. Introduction

Since their discovery in 2011,[1] two-dimensional (2D) metal carbides and nitrides (MXenes) have been extensively studied for various applications.[2-4] Additionally, we envision to expand the application's portfolio of V_2CT_x, especially at high temperature, to areas such as heterogeneous catalysis and/or sensors. In order to do so, new insights on the thermal structure-stability relationships of MXenes are necessary, especially bearing in mind that within the same material, both the chemical and structural properties of the surface and bulk are typically different. Therefore, the utilization of surface/bulk sensitive techniques, especially those allowing *in situ* studies, are highly desired to meticulously study the physicochemical properties of V_2CT_x, and the expanding family of MXene materials in general. The formula for MXenes is $M_{n+1}X_nT_x$, where M is an early transition metal, X is carbon and/or nitrogen, T indicates various surface terminations, *n*=1, 2 or 3, and *x* is the number of surface groups per unit formula.[5] To date, about 20 different MXenes have been synthetized, and many others have been predicted theoretically.[2, 3] The physiochemical properties of these materials primarily depend on their composition and surface terminations (such as F, OH, and/or O), which can be controlled to produce materials with unique properties for specific applications.[3-6] MXenes are produced through selective etching of MAX phases, a family of hexagonal layered ternary carbides and nitrides (with a general formula of $M_{n+1}AX_n$).[5] The synthesis process allows the selective removal of A layered elements (group 13 or 14 elements, i.e. Al) from the structure of MAX phases (i.e. V_2AlC) and the formation of 2D MXenes.[7]

2D MXenes have shown unique electronic, mechanical, and optical properties[8] that render them as promising materials for applications such as gas sensors,[9, 10] water purification,[11] energy storage,[12-15] biosensors,[16] hydrogen and oxygen evolution,[3, 7, 17, 18] and catalysis.[3, 19-22] Particularly V_2CT_x MXene has recently received considerable attention for charge storage applications in lithium-ion and multivalent-ion batteries.[23],[28,14] Up to now, the combination of e*x situ* Raman, X-ray diffraction (XRD), X-ray Photoelectron Spectroscopy (XPS), and Scanning Electron Microscopy (SEM) have been extensively used to characterize the molecular and bulk (crystalline) structure of MXenes, primarily for $Ti_3C_2T_x$.[1, 2, 7, 8, 12, 17, 24-33] In addition, a few *in situ* studies have also been performed using XRD[34] and Raman spectroscopy[35] to study the structure $Ti_3C_2T_x$. Similarly, V_2CT_x has been characterized mainly using *ex situ* XRD, XPS, and SEM,[5, 14, 36-39] and

more recently, Champagne et al^{40} evaluated computationally and experimentally the   Raman spectra of V_2CT_x under ambient conditions.

To the best of our knowledge, in $situ$ characterization of the surface and bulk structure of V_2CT_x, has not yet been performed before, especially under different environments and at temperatures above 25 °C. Therefore, we understand that there are still important insights on the structure-activity-stability relationships of V_2CT_x and MXenes in general to be discovered, discussed, and clarified. As it has been stated in previous studies related to MXenes,[3, 24, 25, 28, 41] their structural stability depend on the chemical environment and the experimental conditions.[3] For instance, ex $situ$ XRD shows that the $Ti_3C_2T_x$ structure is stable at 800-1200 °C under argon [24, 25, 28, 42] although, as suggested by Anasori et $al.,$[3] this still needs to be confirmed by in $situ$ XRD or Raman spectroscopy. In a different study conducted by Zhang et $al.,$[41] ex $situ$ Raman and XRD indicate that Nb_2CT_x oxidizes at 800 °C under CO_2. Nevertheless, a fundamental relationship between the surface and bulk structure with the reactivity of MXenes in operation and under real conditions (in $situ$) still needs to be studied in order to design and prepare MXenes with tunable properties for high temperature applications, such as thermo-catalysis.

Herein, we report on the chemical and thermal stability of V_2CT_x up to 600 °C using in $situ$ Raman spectroscopy, together with ex $situ$ XPS, XRD, and SEM to monitor changes in the surface and the bulk physicochemical properties under different environments (N_2, Air, CO_2, and H_2). By combining ex $situ$ and in $situ$ studies, we demonstrate that the surface transforms differently as compared to the bulk structure as a function of temperature and environment. We primarily concentrate our study on V_2CT_x to identify $i)$ the molecular structure of surface species, due to anticipated thermo-catalytic applications of this material, $ii)$ the structural changes during the dehydration process, and $iii)$ the optimal conditions where the layered structure is preserved. We aim to foster both V_2CT_x and MXenes in general as potential thermo-catalysts, beyond their already proved electro-catalytic applications. Recently, the water gas shift (WGS) reaction at 300 °C and the dehydrogenation of ethylbenzene at 550 °C were experimentally evaluated using Nb_2CT_x and $Ti_3C_2T_x$ MXenes, respectively.[22,43] These reported thermo-catalytic applications validate the importance of our study on establishing qualitative, and soon also quantitative,[44] structure-reactivity relationships for MXenes.

2. Experimental Section

MAX Phase and MXene Synthesis.

Briefly, V_2AlC MAX phase was treated with 48-50% concentrated hydrofluoric acid (ACS grade, BDH) in a ratio of 1g powder to 20 mL etchant for 92 h at room temperature while being stirred with a Teflon-coated magnetic bar at 200 rpm. For more details, the detailed procedure can be found elsewhere.[14] The etched powder was then washed several times using DI water and centrifuged at 3500 rpm for about 5 minutes until the pH of the supernatant was higher than four. The first supernatant after the initial washing step had a green color, indicating dissolvation of vanadium in HF and over-etching of MXene multilayered powders. The MXene powder was then filtered using a Celgard porous membrane, rinsed with DI water and absolute ethanol, collected, and dried under vacuum for 24 h. V_2AlC MAX phase powder with average particle size of less than 32 micron was prepared by mixing elemental powders and high temperature sintering according to previous reports.[14]

Materials Characterization Techniques.

The structure of the synthesized MXene powder was characterized using a Bruker X-ray diffractometer with 40 kV and 40 mA Cu Kα radiation in using 0.2 sec/step. Around 20 mg of sample was loaded in the small cavity of the sample holder and pressed using a glass slide. Cross section morphologies were obtained using JEOL JSM-7000F scanning electron microscope.

Raman spectroscopy studies were performed using a Renishaw InVia Qontor Raman Spectrometer equipped with 785, 532, and 405 nm solid-state lasers, 5, 20, 50, and 100x objectives, and a MS 20 Encoded Stage. *In situ* Raman studies were performed by coupling a Linkam CCR-1000 cell to the Raman microscope. The LiveTrack feature of the Qontor version of the InVia Raman Microscope was used to maintain the sample in focus and, therefore, more accurately correlate changes in the intensity of the Raman signals with specific chemical reactions as a function of time. For *in situ* Raman studies, the samples were treated under inert, reducing, and oxidizing atmospheres using UHP gases in all cases. The various gases were introduced into the Linkam cell at gas hourly space velocity (GHSV) of 36,000 mL $gm^{-1}hr^{-1}$. All measurements were taken with the 405 nm laser, 2400 L mm^{-1} grating, 50x long-distance objective, and, using 40 seconds of exposure time, 50% of power, and 40 accumulations. The behavior of the material under various atmospheres at different temperatures was recorded between 25 to 600 °C at a heating rate

of 10 °C min^{-1}. The accumulation of Raman spectra was obtained under isothermal conditions. For the dehydration measurements, gases coming out of the Linkam cell were analyzed using a MKS Cirrus2 Mass Spectrometer.

XPS data was collected by AXIS Ultra DLD (delay lines detector) X-ray photoelectron spectrometer (XPS) from Kratos Analytical Ltd. The end station consisted of a fast entry load lock, sample treatment chamber (STC), and a sample analysis chamber (SAC). Treated MXene samples were analyzed in SAC under 10^{-9} Torr. A monochromatic Al Kα X-ray source was used as the photon source. High-resolution spectra were obtained for C1s, O1s and V2p using a passing energy of 20 eV. The binding energy shifts due to surface charging were corrected using the C1s level at 284.6 eV. Core level peaks of O1s were deconvoluted by using Gaussian-Lorenzian (20%) peaks.

3. Results and Discussions

In order to circumvent batch effects, about 2.5 grams of the same sample from the same batch was used for this study. Batch effects were considered very important for the present study because during the preparation of V_2CT_x. We noticed that a certain amount of residual carbon impurities are also formed along with the MXene phase due to the over etching of the transition metals. As known, such surface carbonaceous deposits influence the material's thermal and chemical properties to a certain extent, and therefore we decided to use the same batch of MXene material for this study. Moreover, residual carbon complicates the Raman characterization of the VO_x species within the MXene, which is also one of the goals of this study. This is due to the stronger Raman scattering of carbon (D and G Raman peaks at 1351 and 1592 cm^{-1}, respectively). A series of Raman spectra from various batches is shown in the Supporting Information. (**Fig. S1**)

3.1 As prepared V_2CT_x before test

The transformation of the V_2AlC MAX phase into the V_2CT_x MXene phase is confirmed by various techniques as shown in **Fig. 1**. The XRD spectra depicted in **Fig. 1a** shows a peak around 2θ of 8.58° which is assigned to the (0002) plane of V_2CT_x MXene.[3, 5, 14, 32, 36-39] Importantly, the position of this peak tends to slightly shift depending on the amount of confined water that intercalates in between the MXene layers,[23] which in turn may change with varying the synthesis conditions. The small peaks around 2θ of 13.5° and 41.5° indicate the presence of a small
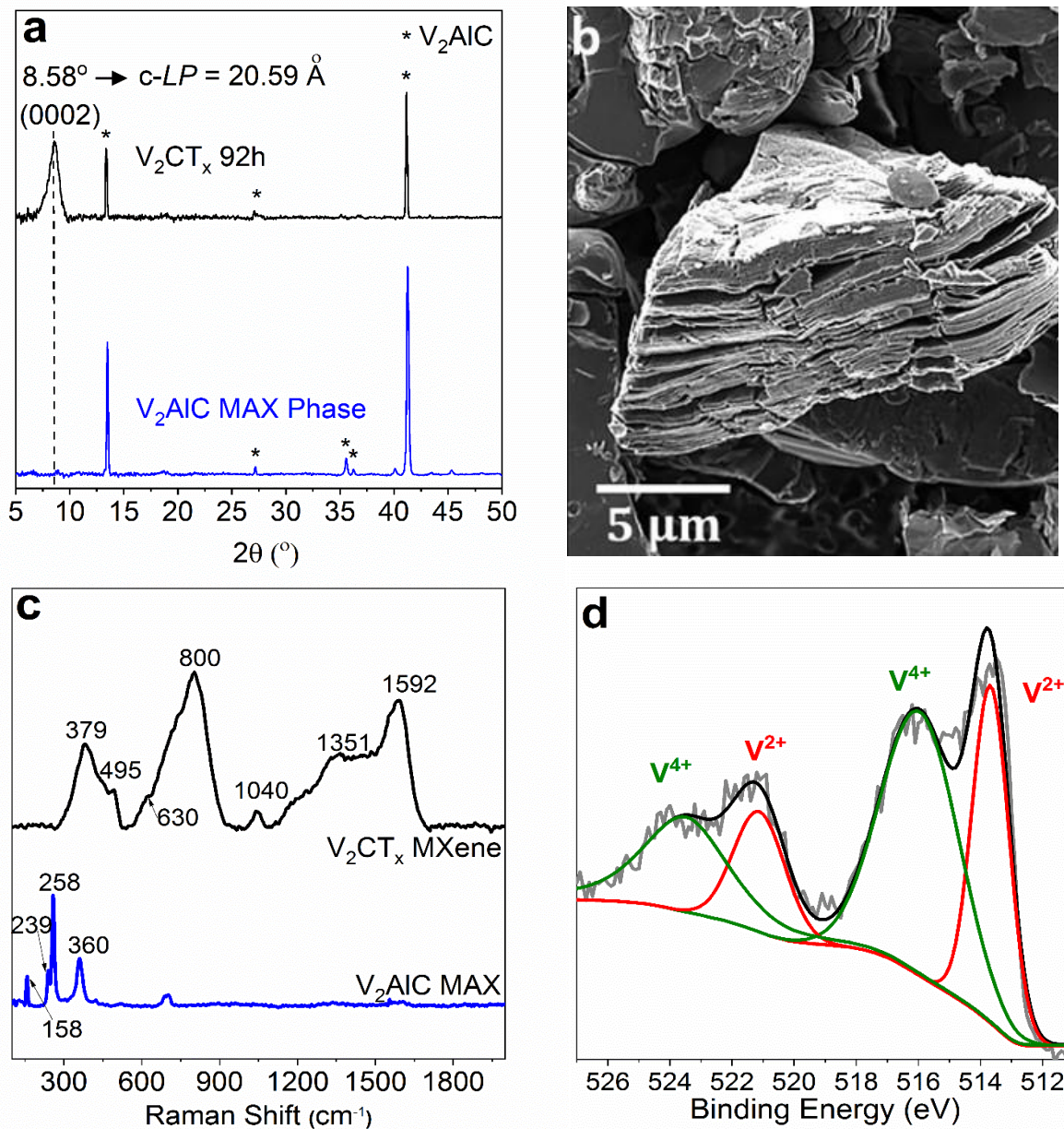
Figure 1. *Ex situ* (a) XRD pattern of V_2CT_x MXene, asterisk (*) denotes unreacted MAX phase (b) SEM image of V_2CT_x MXene. (c) *In situ* Raman spectra (405 nm) for as prepared V_2CT_x MXene and V_2AlC MAX phase, and (d) *ex situ* XPS spectra of V2p region for bare V_2CT_x MXene

amount of unreacted crystalline V_2AlC MAX phase (JCPDS No. 29-0101), consistent with previous reports.[7] This small amount of unreacted MAX phase appears in almost all MXenes

synthesized by HF etching and since it has a more ordered structures compared to the produced MXene, their XRD peaks are relatively sharp.[5, 23] Nevertheless, during our SEM studies almost no MAX particles (similar to before treatment powders) were observed. This indicates that first, the amount of the unreacted particles is very low, and second, the observed sharp XRD peaks most probably originate from partially etched MXene particles which still contain Al. In addition, SEM shows the formation of the typical accordion-like multilayered MXenes structure of V_2CT_x (**Fig. 1b**). The SEM image of V_2AlC MAX is shown in the Supporting Information. (**Fig. S2a**)

After confirming the successful synthesis of V_2CT_x MXenes, *in situ* Raman studies were performed to gain information about the molecular structure of the surface species. **Fig. 1c** shows the Raman spectra for the V_2AlC MAX phase and V_2CT_x MXene. The sharp Raman vibrations observed in the V_2AlC MAX phase transform into broader peaks when it is converted into V_2CT_x MXene. Champagne *et al* suggest that this might happen due to the large interlayer spacing in the MXene phase.[40] The V_2AlC MAX exhibits characteristic Raman peaks at 158, 239, 258, and 360 cm^{-1}.[40, 45, 46] The Raman vibration at 158 and 239 cm^{-1} (E_{2g}) represent in-plane vibration of V and Al atoms, while the vibrations at 258 cm^{-1} (E_{1g}) and 360 cm^1 (A_{1g}) corresponds to the in-plane and out-of-plane vibration of V atoms.[40] On the other hand, V_2CT_x exhibits Raman peaks at 379, 495, and 630 cm^{-1} which are close to those vibrations calculated elsewhere.*[40]* We attribute the Raman vibration around 379 cm^{-1} to A_{1g} (out of plane vibrations of V atoms) mode of V_2C systems, while the Raman vibrations around 495 cm^{-1} to E_g (in plane vibrations of V atoms) mode of $V_2C (OH)_2$ species. [40, 47] The presence of Raman peak in between 400 and 550 cm^{-1} is indicative of terminated V_2CT_x systems and the peak around 630 cm^{-1} correspond to the presence of mixed heterogeneous terminal functionalities (O, F, OH).[40] We performed our Raman study up to longer Raman shift (3000 cm^{-1}) and, therefore, we observed additional peaks. We assign the Raman peak at 800 cm^{-1} to V_2C MXene with terminal functionalities (F, OH), which typically appear below 750 cm^{-1} for V_2C MXene without fluorine and/or hydroxyl terminations.[40] This shift has also been reported for other MXenes.[48]

In addition, we observed a Raman peak at 1040 cm^{-1} attributed to the vanadyl (V=O) stretching for two-dimensional surface VO_x species.[49-52] This Raman V=O vibration corroborates for the first time the two-dimensional nature of VO_x species within the material (typically verified by XRD and SEM). On the other hand, the Raman signals at 1351 and 1592 cm^{-1} are assigned to amorphous (D band) and graphitic (G band) carbon, respectively.[24, 53, 54] These carbon signals

appear due to the over etching of some MXene particles which leads to formation of carbon. It should be noted that previous studies on complete etching of aluminum atoms from MAX phases also show the formation of a mostly amorphous carbon with some graphitic regions.[55]

The XPS spectrum for V2p is shown in **Fig. 1d**. Deconvolution of the V2p region shows the presence of vanadium as V^{2+}(~513.3 eV) and V^{4+} (~516.3 eV), as reported in previous studies.[14] The peak at ~513.3 eV (V^{2+}) shows the presence of unreacted V_2AlC MAX phase and also the contribution from the V-C peak overlap at the same binding energy (~513.3 eV). Therefore the peak is more pronounced considering the strong metal carbide interaction. The peak around ~516.3 eV (V^{4+}) is attributed to the existence of a monolayer of vanadium oxide on the surface of vanadium carbide,[14,23] which corroborates the above-mentioned XRD and Raman results. The XPS spectra for C1s and O1s can be found in the Supporting Information, **Fig. S3**. The C 1s region shows the presence of V-C (~282.2 eV), C-C (~284.8 eV), C-OH (~285.9 eV), and C=O (~288.3 eV), while the O 1s region shows the presence of VO_x (~530 eV), $C-V-O_x$ (~531.2 eV), C-V-(OH) $_x$ (~532 eV) and H_2O_{ads} (~532.2 eV), which we will use for discussion of the V_2CT_x MXenes material when subjected to different chemical atmospheres. The $C-V-O_x$ (~531.2 eV), C-V-(OH) $_x$ (~532 eV) and H_2O_{ads} (~532.2 eV) species comprises majority fraction (~75%) in the O 1s region. The remaining is in the form of mixed vanadium oxide (VO_x) species, which is primarily resulting from surface oxidation. The surface organic contaminants (OR) of COO and C-O contribute in this region, thus overlapping and obscuring other peaks. [56]

3.2 Nitrogen treated V_2CT_x MXene

To determine the thermal stability of V_2CT_x, we exposed it to nitrogen up to 600 °C. As shown in **Fig. 2a**, the intensity of the Raman signals at 800 (carbide phase) and 1040 cm^{-1} (2D V=O) present in the as prepared material remain constant as a function of temperature, proving the thermal stability of V_2CT_x. However, the surface of the material slightly oxidizes at 600 °C as evidenced by the Raman vibration at 450 cm^{-1}. Xie *et al* computationally calculated the activation barriers for dehydration of MXenes and explored the effect of drying temperature on the surface structure.[57] The dehydration follows the Reaction 1, which evidences the change in the surface of MXenes during the dehydration process: [57]
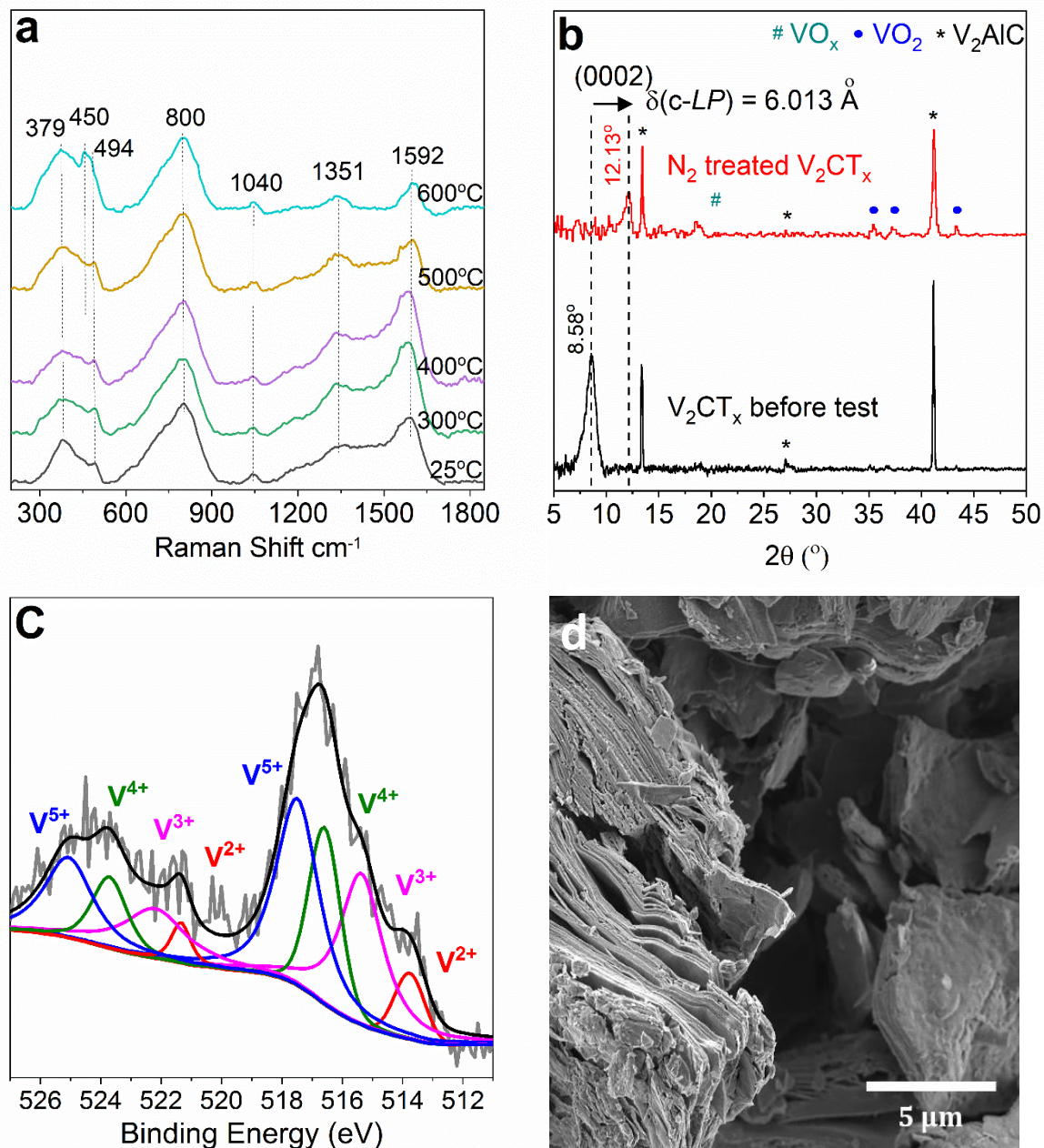
$$M_{n+1}X_n(OH)_2 \rightarrow M_{n+1}X_nO + H_2O \qquad\qquad (1)$$

Figure 2. N2-treated V_2CT_x MXene at 600°C, (a) *In situ* Raman spectra (405 nm), *ex situ* (b) XRD diffractogram, (c) XPS spectra of V2p region, and (d) SEM micrograph

Importantly, we don't find a consensus on the reliable assignment for the Raman vibrations for V_2C with different terminations (F, OH, O). [40, 47] Thus, we ascribe the Raman vibration 450 cm^{-1} to the formation of V_2CO_x species resulting from dehydration of V_2CT_x at high temperature (Reaction 1). The decrease in the intensity of Raman peaks at 1351 (sp[3] amorphous carbon) and

1592 cm^{-1} (sp^2 graphitic carbon) above 500 °C, indicates the gasification of the residual carbon (C + H_2O → CO + H_2) formed due to over etching of V_2CT_x as a product of its reaction with structural water.

In addition, XRD shows a comparison of the as prepared and N_2-treated V_2CT_x at 600 °C (**Fig. 2b**). We attributed the shift of the MXene (0002) peak from 8.58 ° to 12.13 ° due to a decrease in the *c*-LP as a result of the removal of water trapped in-between the layers (dehydration). The formation of small diffraction peaks characteristic for VO_2 (V^{4+}) crystals, confirms the slight peripheral oxidation of material during the dehydration process.

XPS analysis of the V2p region (**Fig. 2c**) reveals the presence of V^{5+} (~517 eV) and V^{3+} (~515.6 eV) along with V^{2+} (~513.3 eV) and V^{4+} (516.3 eV) which were present in the as prepared material, indicating the oxidation of some V^{2+} and V^{4+} species to V^{3+} and V^{5+} species. The presence of V^{5+} species on the outermost layer(s) after the N_2-treatment up to 600 °C, is due to the above-mentioned slight oxidation of the surface vanadium species. The comparison of N_2-treated and the as prepared V_2CT_x, using the C1s and O1s XPS spectra, is shown in the Supporting Information, (**Fig. S4**). The C1s XPS spectrum shows the presence of the V-C (~282.2 eV), C-C (~284.8 eV), C-OH (~285.9 eV), and C=O (~288.3 eV), with a slight decrease in V-C peak. While the O1s spectrum shows the increase in C-V-O_x (~531.2 eV) and C-V-(OH) $_x$ (~532 eV) peak intensity, signaling the miniscule oxidation of the V_2CT_x MXene surface. Finally, SEM-micrograph evidences the persistence of the layered structure of V_2CT_x after the N_2-treatment at 600 °C (**Fig. 2d**). In summary, the bulk structure of V_2CT_x is stable under nitrogen up to 600 °C, while the surface slightly oxides by reacting with the trapped water during the dehydration process.

3.3 Carbon dioxide treated V_2CT_x MXene

Fig. 3 shows the surface and bulk transformation of V_2CT_x MXene under CO_2 at 600 °C. *In situ* Raman spectroscopy (**Fig. 3a**) reveals that as opposed to its behavior under the nitrogen atmosphere, V_2CT_x oxidizes above 300 °C under this mild oxidant gas. First, additional Raman peaks appear at 235 and 332 cm^{-1}, which are assigned to VO_x species, particularly peak around 235 cm^{-1} corresponds to lattice motion involving V-V bonds while around 332 cm^{-1} corresponds to vibrational motion of V-O bonds. [58-61] Second, the Raman peak at 800 cm^{-1} ascribed to vanadium carbide species decreases at temperatures above 400 °C, which does not happen under nitrogen.

This indicates that CO_2 is responsible for this slight oxidation, instead of trapped water. XRD of the CO_2-treated V_2CT_x shows the disappearance of the MXenes peak observed in the as prepared material around 2θ of 8.58° and the advent of new peak around 2θ of 17.01° **(Fig. 3b)**. These peaks are assigned to a formation of VO_x species.[62, 63]
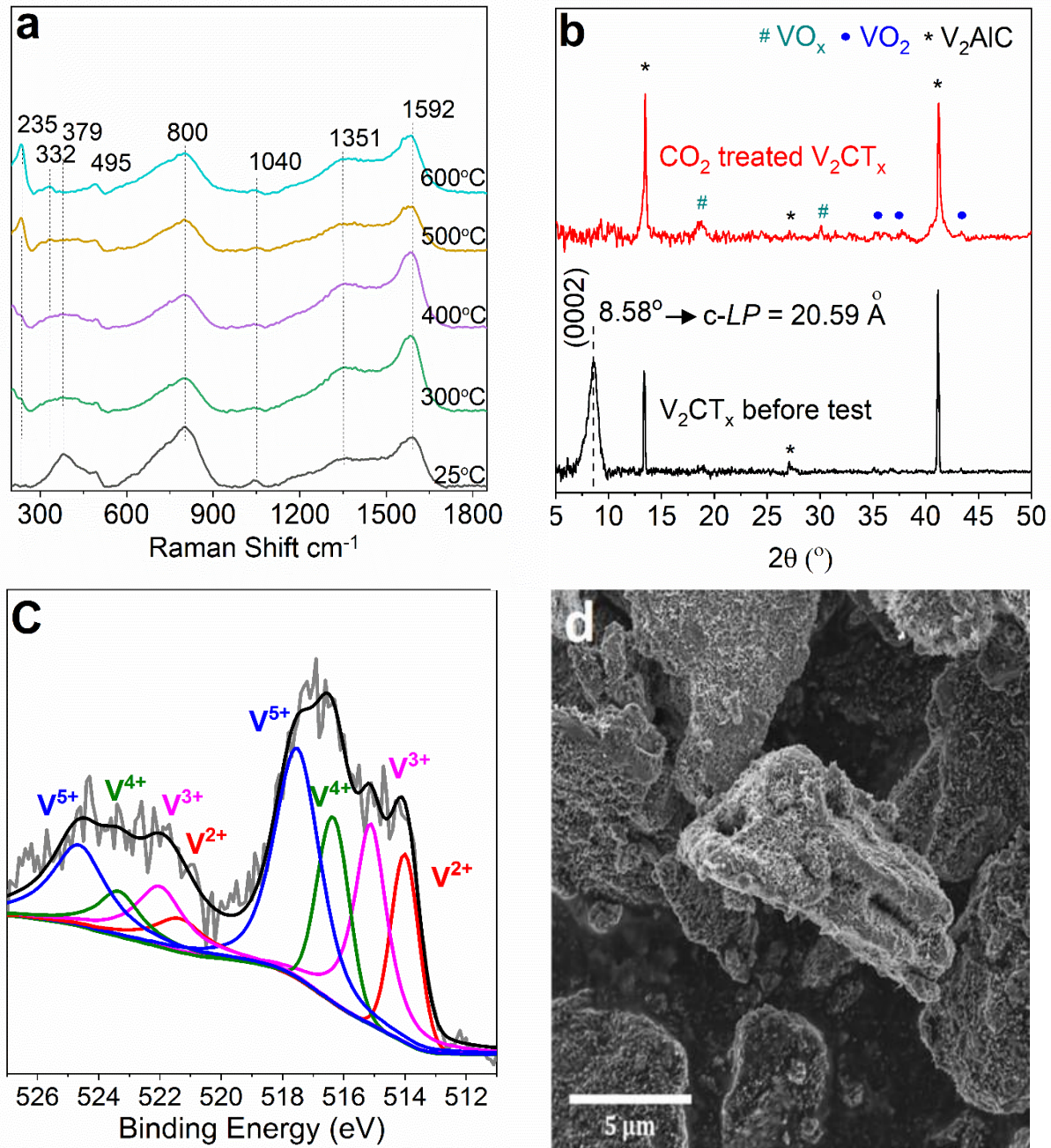

Figure 3. CO_2-treated V_2CT_x MXene at 600°C, (a) *In situ* Raman spectra (405 nm), *ex situ* (b) XRD diffractogram, (c XPS spectra of V2p region, and (d) SEM micrograph

The diffractograms corroborate the slight oxidation of V_2CT_x observed during the *in situ* Raman study (Figure 3a).

XPS analysis of the V2p region **(Fig. 3c)** reveals the presence of V^{5+} (~518 eV) and V^{3+} (~515.6 eV), along with V^{4+} and V^{2+} that are originally present in the as prepared material. This validates the slight surface oxidation of the material due to the presence of CO_2. However, comparing the above-described *in situ* Raman and *ex situ* XRD results, the V_2CT_x surface oxidizes differently to its bulk. The oxidation of the surface is also proven by the decrease in relative intensity in the XPS spectra of the V-C signal at 282.6 eV and the increase in the VO_x (~530 eV), $C-V-O_x$ (~531.2 eV) signals in the O1s region (Supporting Information **Fig. S5**). Finally, SEM studies reveal the formation of homogeneously distributed oxide nanocrystals on the MXene's surface after CO_2-treatment at 600 °C **(Fig. 3d)**. The mild oxidation of the surface and bulk structure of V_2CT_x may favor its electrochemical properties as has already been reported for CO_2-treated Nb_2CT_x MXenes.[41] In addition, SEM reveals the collapse of the layered structure of V_2CT_x, supporting our XRD results.

3.4 Air treated V_2CT_x MXene

Fig. 4 shows the data for V_2CT_X MXene after air-treatment up to 600 °C. *In situ* Raman **(Fig. 4a)** shows the oxidation of V_2CT_X into bulk V_2O_5 around 400 °C as evidenced by *i)* the characteristic V_2O_5 peaks at 294, 480, 520, and 696 cm^{-1},[30, 36-37, 39] *ii)* the shift of the 1040 cm^{-1} peak assigned to the stretching of two-dimensional vanadyl (V=O) species [51, 64] to 995 cm^{-1}, which now corresponds to the stretching of V=O for bulk V_2O_5 particles (supporting information **Fig. S6**)[65, 66] and the disappearance of the peaks at 800, 1351, and 1592 cm^{-1} assigned to the vanadium carbide phase, amorphous sp^3 carbon, and graphitic sp^2 carbon respectively. [40-43]

Additionally, the emergence of sharp XRD peaks around 2θ of 15.4°, 20.3°, 21.75°, 26.17°, 31.0°, 32.4°, 33.36°, 34.32°, 41.32°, and 42.0° (JCPDS No. 41-1426) reveals the oxidation of V_2CT_x into V_2O_5 **(Fig. 4b).** This severe oxidation further leads to the destruction of the layered MXene's structure as shown by the absence of the XRD peak at 2θ of 8.58°. The remaining MAX phase within the MXene material also oxidizes as evidenced by the disappearance of the XRD peak at 2θ of 13.5° while the peak at 41.5° remarkably decreases. For clarification, the XRD spectra of oxidized V_2CT_x MXenes and bulk V_2O_5 can be found in the Supporting Information **(Fig. S7).** XPS analysis of the V2p region **(Fig. 4c)** shows a completely oxidized V_2CT_x surface. Vanadium

is present primarily as V^{5+} (~517 eV), resulting from the oxidation of V^{2+} (513.3 eV) and V^{4+} (516.3 eV) present in the as prepared material (Figure 1b). Additionally, the XPS spectra for C1s and the O1s (Supporting Information, **Fig. S8**) show the disappearance of the V-C peak (~282.6 eV) and the increase in the VO_x species (~530 eV), respectively.
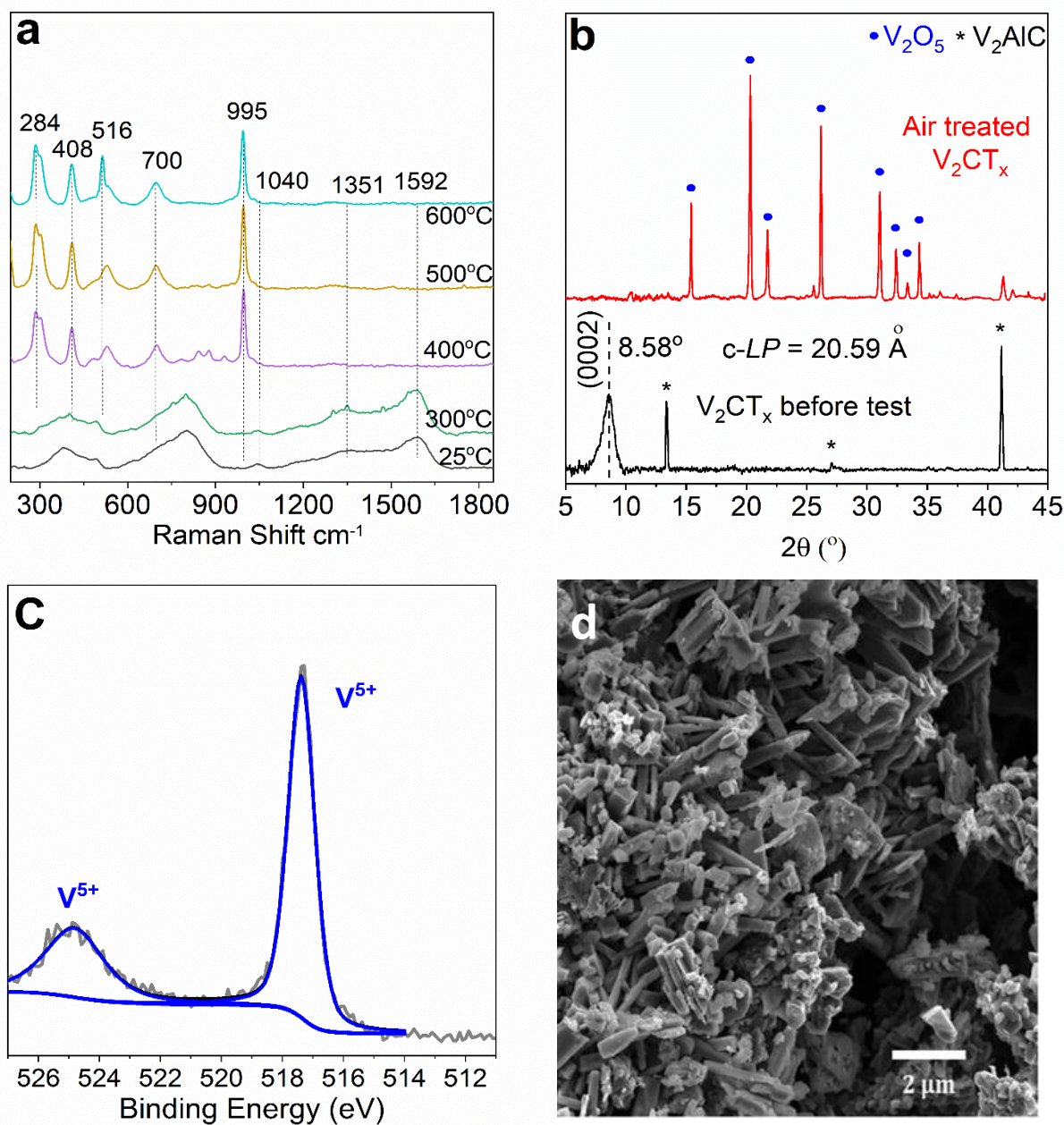

Figure 4. Air-treated V_2CT_x MXene at 600°C, (a) *In situ* Raman spectra (405 nm), *ex situ* (b) XRD diffractogram, (c) XPS spectra of V2p region, and (d) SEM micrograph

Complimentary, SEM was performed to further investigate the structure of the air-treated V_2CT_X MXene at high temperature. The micrograph shows the complete destruction of the layered MXenes structure and the formation of oxide crystals **(Fig. 4d).** These crystals are similar in appearance when compared to the bulk V_2O_5.[67] Thus, the SEM study further substantiate the Raman, XRD, and XPS results discussed above. Similar results was reported for $Ti_3C_2T_x$ MXene and a mechanism for its oxidation as a function of temperature was suggested.[24]

3.5 Hydrogen treated V_2CT_x MXene

As shown in **Fig. 5a**, the decrease in the Raman peaks at 379 and 495 cm^{-1} attributed to A_{1g} (out of plane vibrations of V atoms) mode of V_2C systems and E_g (in plane vibrations of V atoms) mode of $V_2C (OH)_2$ species [40, 47] and in the peak at 1040 cm^{-1} attributed to the stretching of two-dimensional surface vanadyl[65, 66] indicates that reduction of surface vanadium oxide species occurs in the H_2-treated V_2CT_x . Interestingly, the vanadyl Raman peak at 1040 cm^{-1} does not reduce fully, even after 7 hours under reduction, as has been reported for supported two-dimensional vanadium oxide.[68, 69] For clarification, *in situ* Raman spectra highlighting the reduction of the vanadyl group is depicted in the Supporting Information **(Fig. S9).**

The Raman peak at 1592 cm^{-1} assigned to the G carbon band increases as a function of temperature under hydrogen atmosphere (Supporting Information **Fig. S10**). The rise in intensity of G band can be attributed to the loss of surface terminal groups, mainly O and F, from the surface of V_2CT_x exposing the carbon. Similar observations were reported for Ti_2CT_x and Nb_2CT_x MXenes when they were treated under hydrogen environment.[22, 26]

As shown by XRD **(Fig. 5b)**, the MXene peak (0002) for V_2CT_x is no longer observed after reducing the material up to 600 °C. This can be attributed to the removal of water molecules, thus reducing the d-spacing and resulting in the disappearance of MXene peak as the orientation needed for the Bragg's diffraction cannot be formed. Insights on the chemical composition of the surface of the H_2-treated V_2CT_x at 600 °C were gained using XPS **(Fig. 5C)**. Deconvolution of the V2p region of the XPS spectra shows the presence of V^{2+} (~513.3 eV), V^{3+} (~515.8 eV), and V^{4+}

(~516.3 eV), primarily evincing the reduction of the MXene under high temperature hydrogen environment.
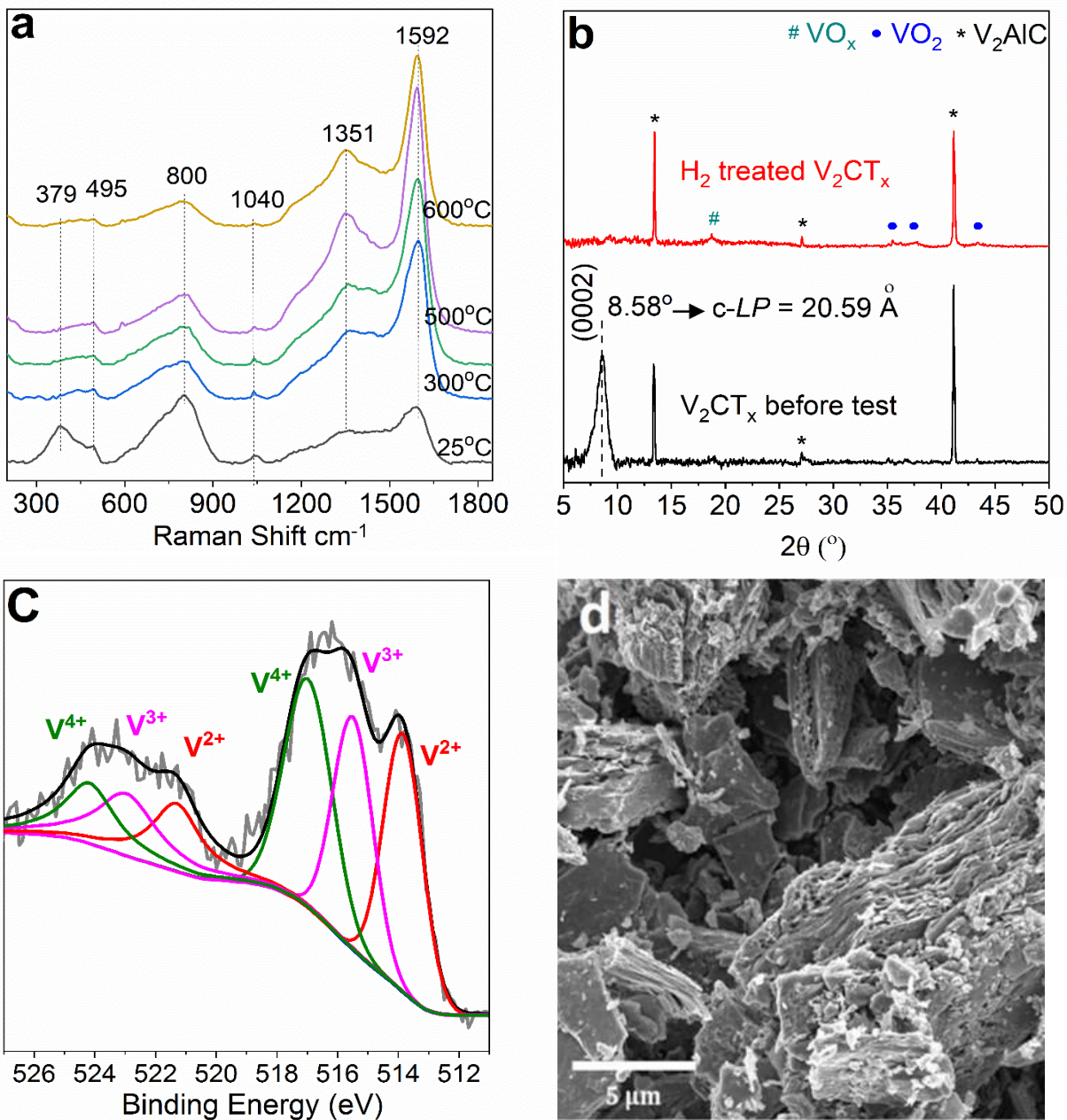

Figure 5. Hydrogen-treated V_2CT_x MXene at 600°C, (a) *In situ* Raman spectra (405 nm), *ex situ* (b) XRD diffractogram, (c) XPS spectra of V2p region, and (d) SEM micrograph

The C1s region still shows the persistence of pronounced V-C (~282.2 eV) peak, thereby indicating the presence of strong metal carbide interaction at the surface (Supporting Information,

Fig. S11). Finally, the SEM micrograph **(Fig. 5d)** reveals the presence of a layered morphology, but with a different structure. Based on the analysis conducted it can be corroborated that the MXene peak (0002) is no longer observed but the layered structure is maintained to a certain degree. The loss of the MXene peak (0002) and difference in the structure is primarily due to the removal of water molecules. Importantly, even after the loss of the MXene peak (0002) layered structure remains to a certain extent after reducing the V_2CT_x for about 7 hours up to 600 °C.

In summary, our data shows that the first chemical and structural transformation of the material from raising the temperature occurs due to the release of the water trapped within the V_2CT_x structure. *In situ* Raman reveals that this dehydration process initiates the partial oxidation of the surface and decreases the distance between the MXene layers above 400 °C. Furthermore, we reveal more insights on the dehydration process of V_2CT_x as shown in **Fig. 6.** It is important to elucidate and understand how water is confined within the MXene material to choose the optimal conditions for dehydration. Multilayered MXenes retain significant amount of water from the existence of hydroxyl groups on the surface and the void volume formed due to the presence of weak hydrogen bonds and van der Waals forces.[70, 71]
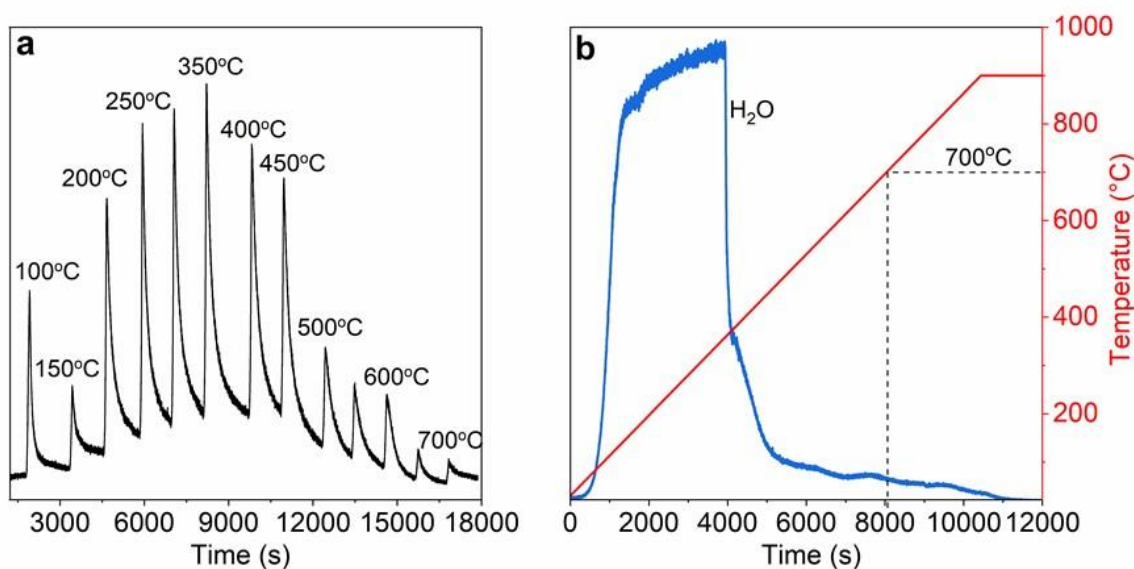

Figure 6. Dehydration of V_2CT_x MXene in (a) 50 °C increments per step up to 700 °C (b) and continuous heating @ 10 °C min^{-1} up to 900 °C

The water adsorbed/trapped between the layers influences the properties of MXenes as it does in other 2D materials such as graphene.[71] When the material is heated up in steps-mode under

nitrogen **(Fig. 6a),** water is released as "*packets*", suggesting that either the water is confined in different compartments within the layered structure or interacting differently with the MXene surface. We hypothesize that the water released up to 150 °C **(Fig. 6a)** represents the adsorbed water on the external surface, while the water trapped in-between the layers starts to desorb above 200 °C.

The water-solid interaction gets stronger, primarily due to the presence of nanoconfined water,[72] therefore more energy is needed to desorb. Most of the water present in V_2CT_x is desorbed once reaching 500 °C **(Fig. 6a)**, however the total dehydration is achieved at about 700 °C, as also shown in **Fig. 6b.** Finally, the partial dehydration of V_2CT_x results in the partial oxidation of the material. Thus, the utilization of V_2CT_x at temperatures between 500 to 700 °C, despite maintaining the multilayered structure, will inevitably lead to the partial oxidation of the material. We believe that our methodology is a unique alternative to tune the dehydration, oxidation, and properties of V_2CTx, which allows for the expansion of MXenes' applications.

4. Conclusions

In this contribution, we provide new insights on the chemical and thermal stability of multilayered V_2CT_x MXene under inert, oxidizing, and reducing environments at various temperatures. Based on our results obtained from *in situ* Raman and *ex situ* XRD, XPS and SEM we listed the most relevant observations as follow:

N_2-treated V_2CT_x:

- The bulk layered structure of the V_2CT_x is stable up to 600 °C, although the surface of the material suffers minor oxidation by reacting with the water intrinsically contained within the structure of the as prepared material.

- The c-LP decreases due to the dehydration of the material, but the layered structure remains intact.

CO_2-treated V_2CT_x:

- The material oxidizes above 300 °C, forming a mixture of VO_x species.

- The bulk layered structure collapses.

Air-treated V_2CT_x:

- The material transforms into bulk V_2O_5 with complete desertion of the characteristic layered structure above 300 °C.

H_2-treated V_2CT_x:

- The bulk layered structure is maintained to a certain degree, although the MXene peak (0002) disappears due to removal of water molecules.

- The surface VO_x species are reduced.

- Terminal functional groups (OH, O and F) gets removed above 300 °C.

Our results indicate that at higher temperatures, the trapped water within the layered structure of the material inevitable burns the residual carbon and slightly oxidizes the V_2CT_x surface (above 400 °C), no matter the environment. This limits the utilization of V_2CT_x for high temperature applications especially when the carbide species, instead of oxi-carbide, are rather needed. However, one can adjust the oxidation degree of the material by tuning the dehydration temperature considering the fact that the water-solid interaction varies depending on the location of the water (trapped water). In fact, we foresee that when working at lower temperatures, and especially under reducing atmospheres, V_2CT_x will exhibit unprecedented thermo-catalytic properties. Additionally, the collapse of the MXene structure and the formation of different surface/bulk oxide and oxi-carbide species foster V_2CT_x and MXenes in general as a potential precursor for new bulk V_2O_5 and/or $V_xO_yC_z$ (oxi-carbide) catalysts. In our on-going studies we are using the chemical and thermal properties of V_2CT_x presented in this work to select the optimal reaction conditions to perform various industrially attractive thermo-catalytic reactions. An important challenge we identified in this study is the irreversibility of the destruction and/or oxidation of the layered (accordion-type) structure. In order to broaden the applications of MXenes, especially at higher temperatures and under oxidizing atmospheres, we might both enhance the stability of these materials towards oxidation and, more importantly, we need to develop methodologies to synthesize MAX phase and, therefore, MXene phase starting from a collapsed/oxidized material.

ACKNOWLEDGMENTS

Conflict of Interest

The authors declare no conflict of interest.

Supporting Information

Supporting information is available from the Wiley Online Library or from the authors.

REFERENCES

1. M. Naguib, M. Kurtoglu, V. Presser, J. Lu, J. Niu, M. Heon, L. Hultman, Y. Gogotsi and M. W. Barsoum, *Advanced Materials*, 2011, **23**, 4248-4253.
2. J. Zhu, E. Ha, G. Zhao, Y. Zhou, D. Huang, G. Yue, L. Hu, N. Sun, Y. Wang, L. Y. S. Lee, C. Xu, K.-Y. Wong, D. Astruc and P. Zhao, *Coordination Chemistry Reviews*, 2017, **352**, 306-327.
3. B. Anasori, M. R. Lukatskaya and Y. Gogotsi, *Nature Reviews Materials*, 2017, **2**, 16098.
4. Y. Gogotsi, *Nanomaterials handbook*, CRC press, 2006.
5. M. Naguib, V. N. Mochalin, M. W. Barsoum and Y. Gogotsi, *Adv Mater*, 2014, **26**, 992-1005.
6. B. Anasori, Y. Xie, M. Beidaghi, J. Lu, B. C. Hosler, L. Hultman, P. R. Kent, Y. Gogotsi and M. W. Barsoum, *ACS nano*, 2015, **9**, 9507-9516.
7. M. Naguib, O. Mashtalir, J. Carle, V. Presser, J. Lu, L. Hultman, Y. Gogotsi and M. W. Barsoum, *ACS Nano*, 2012, **6**, 1322-1331.
8. B. Akuzum, K. Maleski, B. Anasori, P. Lelyukh, N. J. Alvarez, E. C. Kumbur and Y. Gogotsi, *ACS nano*, 2018, **12**, 2685-2694.
9. E. Lee, A. VahidMohammadi, B. C. Prorok, Y. S. Yoon, M. Beidaghi and D.-J. Kim, *ACS applied materials & interfaces*, 2017, **9**, 37184-37190.

10. S. J. Kim, H.-J. Koh, C. E. Ren, O. Kwon, K. Maleski, S.-Y. Cho, B. Anasori, C.-K. Kim, Y.-K. Choi and J. Kim, *ACS nano*, 2018, **12**, 986-993.

11. Q. Zhang, J. Teng, G. Zou, Q. Peng, Q. Du, T. Jiao and J. Xiang, *Nanoscale*, 2016, **8**, 7085-7093.

12. Y.-Y. Peng, B. Akuzum, N. Kurra, M.-Q. Zhao, M. Alhabeb, B. Anasori, E. C. Kumbur, H. N. Alshareef, M.-D. Ger and Y. Gogotsi, *Energy & Environmental Science*, 2016, **9**, 2847-2854.

13. C. Couly, M. Alhabeb, K. L. Van Aken, N. Kurra, L. Gomes, A. M. Navarro-Suárez, B. Anasori, H. N. Alshareef and Y. Gogotsi, *Advanced Electronic Materials*, 2018, **4**, 1700339.

14. A. VahidMohammadi, A. Hadjikhani, S. Shahbazmohamadi and M. Beidaghi, *ACS Nano*, 2017, **11**, 11135-11144.

15. A. VahidMohammadi, J. Moncada, H. Chen, E. Kayali, J. Orangi, C. A. Carrero and M. Beidaghi, *Journal of Materials Chemistry A*, 2018.

16. B. Xu, M. Zhu, W. Zhang, X. Zhen, Z. Pei, Q. Xue, C. Zhi and P. Shi, *Advanced Materials*, 2016, **28**, 3333-3339.

17. V. M. Hong Ng, H. Huang, K. Zhou, P. S. Lee, W. Que, J. Z. Xu and L. B. Kong, *Journal of Materials Chemistry A*, 2017, **5**, 3039-3068.

18. W. Choi, N. Choudhary, G. H. Han, J. Park, D. Akinwande and Y. H. Lee, *Materials Today*, 2017, **20**, 116-130.

19. Y. Gao, L. Wang, Z. Li, A. Zhou, Q. Hu and X. Cao, *Solid State Sciences*, 2014, **35**, 62-65.

20. L. M. Azofra, N. Li, D. R. MacFarlane and C. Sun, *Energy & Environmental Science*, 2016, **9**, 2545-2549.

21. X. Zhang, J. Lei, D. Wu, X. Zhao, Y. Jing and Z. Zhou, *Journal of Materials Chemistry A*, 2016, **4**, 4871-4876.

22. Z. Li, Y. Cui, Z. Wu, C. Milligan, L. Zhou, G. Mitchell, B. Xu, E. Shi, J. T. Miller and F. H. Ribeiro, *Nature Catalysis*, 2018, 1.

23. M. Naguib, J. Halim, J. Lu, K. M. Cook, L. Hultman, Y. Gogotsi and M. W. Barsoum, *Journal of the American Chemical Society*, 2013, **135**, 15966-15969.

24. H. Ghassemi, W. Harlow, O. Mashtalir, M. Beidaghi, M. R. Lukatskaya, Y. Gogotsi and M. L. Taheri, *Journal of Materials Chemistry A*, 2014, **2**, 14339-14343.

25. S. Lai, J. Jeon, S. K. Jang, J. Xu, Y. J. Choi, J.-H. Park, E. Hwang and S. Lee, *Nanoscale*, 2015, **7**, 19390-19396.

26. R. Rakhi, B. Ahmed, M. N. Hedhili, D. H. Anjum and H. N. Alshareef, *Chemistry of Materials*, 2015, **27**, 5314-5323.

27. H. Wang, Y. Wu, J. Zhang, G. Li, H. Huang, X. Zhang and Q. Jiang, *Materials Letters*, 2015, **160**, 537-540.

28. K. Wang, Y. Zhou, W. Xu, D. Huang, Z. Wang and M. Hong, *Ceramics International*, 2016, **42**, 8419-8424.

29. Y. Cai, J. Shen, G. Ge, Y. Zhang, W. Jin, W. Huang, J. Shao, J. Yang and X. Dong, *ACS nano*, 2017.

30. A. Feng, Y. Yu, F. Jiang, Y. Wang, L. Mi, Y. Yu and L. Song, *Ceramics International*, 2017, **43**, 6322-6328.

31. M. Khazaei, A. Ranjbar, M. Arai, T. Sasaki and S. Yunoki, *Journal of Materials Chemistry C*, 2017, **5**, 2488-2503.

32.   R. Li, L. Zhang, L. Shi and P. Wang, *ACS Nano*, 2017, **11**, 3752-3759.
33.   C. J. Zhang, S. Pinilla, N. McEvoy, C. P. Cullen, B. Anasori, E. Long, S.-H. Park, A. Seral-Ascaso, A. Shmeliov, D. Krishnan, C. Morant, X. Liu, G. S. Duesberg, Y. Gogotsi and V. Nicolosi, *Chemistry of Materials*, 2017, **29**, 4848-4856.
34.   Z. Lin, P. Rozier, B. Duployer, P.-L. Taberna, B. Anasori, Y. Gogotsi and P. Simon, *Electrochemistry Communications*, 2016, **72**, 50-53.
35.   M. Hu, Z. Li, T. Hu, S. Zhu, C. Zhang and X. Wang, *ACS nano*, 2016, **10**, 11344-11350.
36.   D. Sun, Q. Hu, J. Chen, X. Zhang, L. Wang, Q. Wu and A. Zhou, *ACS applied materials & interfaces*, 2015, **8**, 74-81.
37.   F. Liu, J. Zhou, S. Wang, B. Wang, C. Shen, L. Wang, Q. Hu, Q. Huang and A. Zhou, *Journal of The Electrochemical Society*, 2017, **164**, A709-A713.
38.   Y. Dall'Agnese, P. L. Taberna, Y. Gogotsi and P. Simon, *J Phys Chem Lett*, 2015, **6**, 2305-2309.
39.   S.-M. Bak, R. Qiao, W. Yang, S. Lee, X. Yu, B. Anasori, H. Lee, Y. Gogotsi and X.-Q. Yang, *Advanced Energy Materials*, 2017, **7**, 1700959.
40.   A. Champagne, L. Shi, T. Ouisse, B. Hackens and J.-C. Charlier, *Physical Review B*, 2018, **97**, 115439.
41.   C. Zhang, M. Beidaghi, M. Naguib, M. R. Lukatskaya, M.-Q. Zhao, B. Dyatkin, K. M. Cook, S. J. Kim, B. Eng and X. Xiao, *Chemistry of Materials*, 2016, **28**, 3937-3943.
42.   C. E. Ren, K. B. Hatzell, M. Alhabeb, Z. Ling, K. A. Mahmoud and Y. Gogotsi, *The journal of physical chemistry letters*, 2015, **6**, 4026-4031.
43.   J. Diao, M. Hu, Z. Lian, Z. Li, H. Zhang, F. Huang, B. Li, X. Wang, D. Su and H. Liu, *ACS Catalysis*, 2018.
44.   J. Moncada, W. R. Adams, R. Thakur, M. Julin and C. A. Carrero, *ACS Catalysis*, 2018.
45.   V. Presser, M. Naguib, L. Chaput, A. Togo, G. Hug and M. W. Barsoum, *Journal of Raman Spectroscopy*, 2012, **43**, 168-172.
46.   J. E. Spanier, S. Gupta, M. Amer and M. W. Barsoum, *Physical Review B*, 2005, **71**, 012103.
47.   M. Wu, B. Wang, Q. Hu, L. Wang and A. Zhou, *Materials*, 2018, **11**, 2112.
48.   U. Yorulmaz, A. Özden, N. K. Perkgöz, F. Ay and C. Sevik, *Nanotechnology*, 2016, **27**, 335702.
49.   G. T. Went, S. T. Oyama and A. T. Bell, *Journal of physical chemistry*, 1990, **94**, 4240-4246.
50.   B. Olthof, A. Khodakov, A. T. Bell and E. Iglesia, *The Journal of Physical Chemistry B*, 2000, **104**, 1516-1528.
51.   C. Carrero, R. Schlögl, I. Wachs and R. Schomaecker, *Acs Catalysis*, 2014, **4**, 3357-3380.
52.   I. E. Wachs and B. M. Weckhuysen, *Applied Catalysis A: General*, 1997, **157**, 67-90.
53.   M. S. Dresselhaus, A. Jorio, M. Hofmann, G. Dresselhaus and R. Saito, *Nano letters*, 2010, **10**, 751-758.
54.   M. S. Dresselhaus, G. Dresselhaus, R. Saito and A. Jorio, *Physics reports*, 2005, **409**, 47-99.
55.   M. R. Lukatskaya, J. Halim, B. Dyatkin, M. Naguib, Y. S. Buranova, M. W. Barsoum and Y. Gogotsi, *Angewandte Chemie International Edition*, 2014, **53**, 4877-4880.
56.   J.-G. Choi, *Applied surface science*, 1999, **148**, 64-72.

57.   Y. Xie, M. Naguib, V. N. Mochalin, M. W. Barsoum, Y. Gogotsi, X. Yu, K.-W. Nam, X.-Q. Yang, A. I. Kolesnikov and P. R. Kent, *Journal of the American Chemical Society*, 2014, **136**, 6385-6394.

58.   X. B. Chen, J. H. Shin, H. T. Kim and Y. S. Lim, *Journal of Raman Spectroscopy*, 2012, **43**, 2025-2028.

59.   G. Petrov, V. Yakovlev and J. Squier, *Applied physics letters*, 2002, **81**, 1023-1025.

60.   Y. Hong-Tao, F. Ke-Cheng, W. Xue-Jin, L. Chao, H. Chen-Juan and N. Yu-Xin, *Chinese Physics*, 2004, **13**, 82.

61.   F. Ureña-Begara, A. Crunteanu and J.-P. Raskin, *Applied Surface Science*, 2017, **403**, 717-727.

62.   P. Phoempoon and L. Sikong, *The Scientific World Journal*, 2014, **2014**.

63.   C. Wu, F. Feng and Y. Xie, *Chemical Society Reviews*, 2013, **42**, 5157-5183.

64.   J. T. Grant, C. A. Carrero, A. M. Love, R. Verel and I. Hermans, *ACS Catalysis*, 2015, **5**, 5787-5793.

65.   C. A. Carrero, C. J. Keturakis, A. Orrego, R. Schomacker and I. E. Wachs, *Dalton Trans*, 2013, **42**, 12644-12653.

66.   C. A. Carrero, S. P. Burt, F. Huang, J. M. Venegas, A. M. Love, P. Mueller, H. Zhu, J. T. Grant, R. Mathison and M. P. Hanraham, *Catalysis Science & Technology*, 2017, **7**, 3707-3714.

67.   A. Sakunthala, M. Reddy, S. Selvasekarapandian, B. Chowdari and P. C. Selvin, *Energy & Environmental Science*, 2011, **4**, 1712-1725.

68.   Z. J. Zhao, T. Wu, C. Xiong, G. Sun, R. Mu, L. Zeng and J. Gong, *Angewandte Chemie International Edition*, 2018, **57**, 6791-6795.

69.   G. Liu, Z.-J. Zhao, T. Wu, L. Zeng and J. Gong, *ACS Catalysis*, 2016, **6**, 5207-5214.

70.   N. C. Osti, A. Cote, E. Mamontov, A. Ramirez-Cuesta, D. Wesolowski and S. Diallo, *Chemical Physics*, 2016, **465**, 1-8.

71.   N. C. Osti, M. Naguib, A. Ostadhossein, Y. Xie, P. R. Kent, B. Dyatkin, G. Rother, W. T. Heller, A. C. Van Duin and Y. Gogotsi, *ACS applied materials & interfaces*, 2016, **8**, 8859-8863.

72.   N. Shpigel, M. D. Levi, S. Sigalov, T. S. Mathis, Y. Gogotsi and D. Aurbach, *Journal of the American Chemical Society*, 2018.

Graphical Abstract

V_2CT_x exposed to N_2, CO_2, Air, and H_2 at elevated temperatures